

# Prediction of topological superconductivity in Mn-doped GeTe monolayer from first-principles

Xiaoming Zhang<sup>1,2,3</sup>, Kyung-Hwan Jin<sup>4,3</sup>, Jiahao Mao<sup>5</sup>, Mingwen Zhao<sup>6</sup>, Zheng Liu<sup>2\*</sup>,  
and Feng Liu<sup>3\*</sup>

<sup>1</sup> *College of Information Science and Engineering, Ocean University of China,  
Qingdao, Shandong 266100, China*

<sup>2</sup> *Institute for Advanced Study, Tsinghua University, Beijing 100084, China*

<sup>3</sup> *Department of Materials Science and Engineering, University of Utah, Salt Lake  
City, Utah 84112, USA*

<sup>4</sup> *Department of Physics, Pohang University of Science and Technology, Pohang  
37673, Republic of Korea*

<sup>5</sup> *State Key Laboratory of Low Dimensional Quantum Physics and Department of  
Physics, Tsinghua University, Beijing, 100084, China*

<sup>6</sup> *School of Physics and State Key Laboratory of Crystal Materials, Shandong  
University, Jinan, Shandong 250100, China*

\*Correspondence to: [fliu@eng.utah.edu](mailto:fliu@eng.utah.edu), [zheng-liu@mail.tsinghua.edu.cn](mailto:zheng-liu@mail.tsinghua.edu.cn)

The discovery of signatures of topological superconductivity (TSC) in several material systems has sparked enormous research interests. The realization of TSC typically requires a delicate tuning of multiple microscopic parameters, which remains a great experimental challenge. Here, by determining term-by-term the band dispersion with spin-orbit coupling, Zeeman splitting and electron-phonon coupling strength, we demonstrate a systematic first-principles approach to quantify the realistic conditions of TSC, which combines Wannier function construction with a self-consistent solution of Bogoliubov-de Gennes (BdG) equation. We choose the Mn-doped GeTe ( $\text{Ge}_{1-x}\text{Mn}_x\text{Te}$ ) monolayer – a well-studied dilute magnetic semiconductor showing superconductivity under hole doping – as an example to construct a first-principles phase diagram. A Class D TSC phase, with the Chern number of 1 and optimal transition temperature of  $\sim 2.8$  K, is predicted to occur within the Mn concentration  $x \sim (0.002, 0.025)$  and hole concentration  $\sim 7.4 \times 10^{13} \text{ cm}^{-2}$ . Our computational approach can be applied to other TSC schemes with a phonon-mediated pairing, e.g. doped topological insulators and Fu-Kane heterostructures, providing a quantitative guidance for future experimental studies.

*Introduction.*—The topological phase of superconductors (SC) has recently received intense research interests because the superconducting quasiparticles residing in the non-trivial gapless/zero-energy boundary states are considered a form of Majorana fermions. Majorana fermions are their own anti-particles [1] and obey the non-Abelian exchange statistics, [2,3] which can be utilized for topological quantum computation.[4,5] Topological superconductors (TSC) exhibit various exotic phenomena, including zero modes on the magnetic vortex, [6] “fractional” Josephson effect, [7,8] non-local correlation, [9,10] and thermal responses. [11-13] By now, the theoretical aspects of TSCs are reasonably well understood, but the experimental confirmation remains a great challenge due to the requirement of tuning multiple microscopic parameters like the Fermi level, magnetic field, temperature, etc.. Hence, it is highly desirable to predict more TSCs and quantify experimental conditions to advance the field.

Generally, TSCs can be classified as intrinsic or artificial, depending on the origin of nontrivial superconducting gap. [14,15] It has been proposed to realize intrinsic TSCs in  $p$ -wave SCs, such as  $\text{Sr}_2\text{RuO}_4$ , [16,17] the Cu/Sr/Nb-doped  $\text{Bi}_2\text{Se}_3$ [18] and non-centrosymmetric SCs, [19,20] which are natural consequence of spin-triplet pairing. [21,22] Differently, artificial TSCs, e.g. Class D TSCs, may stem from spin-singlet pairing combined with helical spin-polarized states and time-reversal symmetry breaking, as proposed by theoretical models based on non-degenerate two-dimensional (2D) Dirac fermions, [23,24] as well as 1D [25,26] and 2D Rashba electrons [27-29]. Through superconducting proximity effect, the former two models have been experimentally realized in topological surface states [30-33] and in semiconductor nanowires with strong spin-orbit coupling (SOC) [34], respectively. Also, it was theoretically suggested that Class D TSCs may be engineered in ultrathin superconducting films on a substrate. [35,36] In-gap states at  $\text{SrTiO}_3/\text{LaAlO}_3$  interface [37] and in Bi/Ni bilayer [38] have been observed, but the physical origin of the zero-bias anomaly remains controversial [37-46].

Unlike the successful first-principles prediction of electronic and topological materials, theoretical predictions of TSCs are challenging because of the uncertainty in the parameters used to construct Bogoliubov-de Gennes (BdG) Hamiltonian. Usually, only the pre-conditions of TSC, e.g. Rashba splitting [36] or topological properties [47-50] in the normal state of known superconductors, were analyzed using first-principles method, but not the topology of superconducting quasiparticles. Instead, effective models of TSC states are constructed with empirical parameters, at the best partially fit to the first-principles results. [51,52]

Here, we attempt to extend first-principles calculations to the field of TSCs by constructing a material-specific first-principles BdG Hamiltonian. Given the necessary conditions for realizing Class D TSCs with 2D Rashba electrons, [27-29] i.e. inversion symmetry breaking, Zeeman gap opening and superconductivity, the IV-VI compound germanium telluride (GeTe), a dilute magnetic semiconductors (DMS) with a ferromagnetic Curie temperatures  $T_c^{\text{FM}}$  of  $\sim 150$  K for bulk [53] and up to  $\sim 200$  K for

epitaxial layers on BaF<sub>2</sub> (111) substrate, [54-58] caught our attention. The superconductivity of GeTe with *p*-type doping due to Ge vacancy was confirmed as early as the 1960s. [59,60] It is also known as a ferroelectric material with rhombohedral layered, non-centrosymmetric structure below the ferroelectric Curie temperature of ~700 K. [61,62] Recently, a gradual opening of Zeeman gap in the Rashba bands of GeTe with Mn doping was observed, attributed to the entanglement of ferromagnetic and ferroelectric order. [63,64]

Specifically, we focus on the recent experimentally exfoliated GeTe monolayer, [65] which was predicted to be useful in optoelectronic devices and may be a type-II Ising superconductor upon slight hole doping. [66,67] Using first-principles calculations, we show that GeTe monolayer inherits all the key characteristics of its bulk phase, including the Zeeman gap opening upon Mn doping. The computational details are presented in the Supplemental Material (SM). [68] The first-principles BdG Hamiltonian was constructed via a Wannier-function scheme, through which we found that the 0.1-hole-doped GeTe monolayer is a two-gap ( $\Delta_s \sim 0.276$  and  $\sim 0.603$  meV) *s*-wave superconductor and the Ge<sub>1-x</sub>Mn<sub>x</sub>Te monolayer is a Class D TSC characterized by a non-zero Chern number. A phase diagram of Ge<sub>1-x</sub>Mn<sub>x</sub>Te is constructed to guide experimental detection of the predicted SC and TSC phase. Since both the exfoliated GeTe monolayer and epitaxial Ge<sub>1-x</sub>Mn<sub>x</sub>Te thin film already exist [54-58], our prediction should be readily testable experimentally. Our approach also provides a benchmark to make material-specific predictions of TSCs by using first-principles calculations.

*Crystal and electronic band structure.*—The crystal structure of GeTe monolayer is shown in Fig. 1a, which is a [111] layer fragment of its bulk phase. Each Ge(Te) atom is bonded with three Te(Ge) atoms, forming a buckled honeycomb lattice. The in-plane lattice constant *a* and buckling height *h* was optimized to be  $\sim 3.955$  Å and  $\sim 1.565$  Å, respectively, in good agreement with previous report. [66] Due to the absence of inversion symmetry, a large Rashba splitting arises in the electronic band structure considering SOC (Fig. 1b). The electronic states are doubly degenerate at the  $\Gamma$  and M points, forming the so-called Kramers pairs, while the degeneracy was lifted away from these time-reversal invariant points. For the four bands near the Fermi level of our interest, hereafter we name the lower (upper) two bands as the inner (outer) bands for clarity.

To predict the TSC formed by 2D Rashba electrons, [27-29] we focus on the inner bands with a significant Rashba splitting coefficient  $\alpha_R = 0.66\sim 0.76$  eV Å. It is comparable with that of heavy metals Au(111) and Bi(111) surface, [69-71] but slightly smaller than that of bulk GeTe. [72,73] A strong Rashba effect is desirable for the electrons to overcome the suppressing effect of Zeeman field on superconductivity. [74] Doping 0.1 holes per primitive cell will move the Fermi level to the Dirac point formed by Rashba splitting (Fig. 1b), which corresponds to a hole concentration of  $\sim 7.4 \times 10^{13}$  cm<sup>-2</sup>. The electronic density of states (DOS)  $N_F$  at the Fermi level ( $E_F$ ) is increased from 0 to  $\sim 1.04$  states/eV/primitive-cell, which stems mainly from the *p*-orbitals of Te and

Ge atoms (Fig. S1). Figure 1c shows the spin-texture  $s(\mathbf{k})$  on the Fermi surfaces (FSs) of the 0.1-hole-doped GeTe monolayer. One can clearly see the in-plane components are helical-like, while the out-of-plane ones are small. The metallic nature and the anti-parallel spins at the  $\mathbf{k}$  and  $-\mathbf{k}$  points provide the prerequisite conditions for s-wave superconductivity.

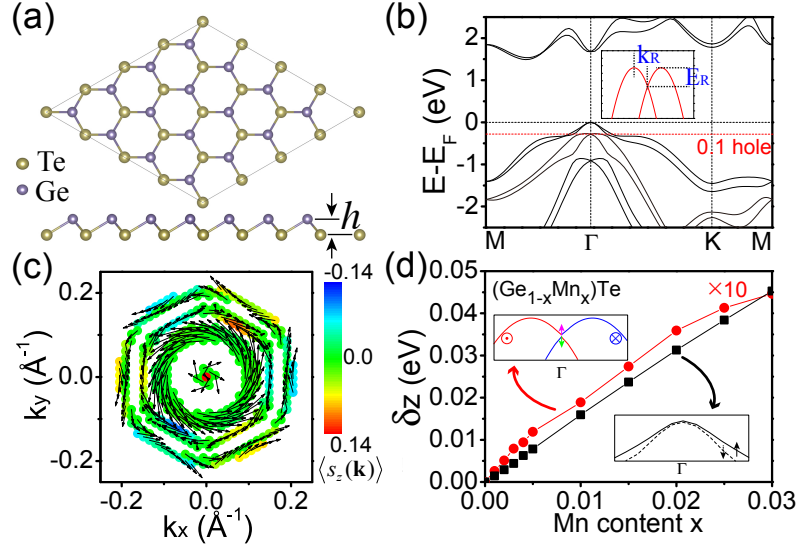


**Figure 1.** (a) The top and side view of GeTe monolayer and (b) its electronic band structure. The black horizontal dashed line represents the Fermi level and the red one is the Fermi level after doping 0.1 holes per primitive cell. Inset shows the momentum offset  $k_R$  and the energy splitting  $E_R$  used for calculating the Rashba splitting coefficient  $\alpha_R = 2E_R/k_R$ . (c) The electronic spin-texture on the FS of the 0.1-hole-doped GeTe monolayer (d) The Zeeman gaps ( $\delta_z$ ) of  $\text{Ge}_{1-x}\text{Mn}_x\text{Te}$  monolayer versus the concentration  $x$  of Mn dopants with high-spin state ( $S_{\text{Mn}}=5/2$ ). Black filled squares represent the  $\delta_z$  opened at the VBM, and the red dots represent the  $\delta_z$  (magnified by 10) opened at the Dirac point formed by Rashba splitting. Insets are the schematic diagrams for the electronic spins near the VBM (bottom-right inset) and Dirac point (top-left inset).

Having demonstrated the Rashba spin splitting in the GeTe monolayer, we now discuss the second ingredient, the Zeeman gap. It has been reported that a Zeeman gap can be opened in the bulk  $\text{Ge}_{1-x}\text{Mn}_x\text{Te}$  with a ferromagnetic order parallel to the [111] direction [63,64], which is the easy magnetization direction for small  $x$  [75]. Since two possible spin states of Mn atoms (high-spin state,  $S=5/2$ , and intermediate-spin state,  $S=3/2$ ) exist under different conditions [76], it is necessary to determine the most favorable state in  $\text{Ge}_{1-x}\text{Mn}_x\text{Te}$ . Based on the virtual crystal approximation (VCA) [77], the calculated Zeeman gaps of bulk  $\text{Ge}_{1-x}\text{Mn}_x\text{Te}$  show similar trends with the experimental report [63] for both high- and intermediate-spin states (Fig. S2), [68] but the former one appears to reproduce the experimental results better for  $x < 0.06$ . This indicates the doped Mn atom is in  $\text{Mn}^{2+}$  state, consistent with previous experimental reports [53,56,78]. The slight deviation among them may be attributed to the

antiferromagnetic coupling between the randomly distributed nearest-neighbor Mn dopants in experimental samples [79]. At higher Mn concentration, reorientation of the easy magnetization axis from the normal of [111] surface towards the in-plane direction may occur [75].

Consequently, the out-of-plane high-spin state ( $S=5/2$ ) of Mn dopants is adopted in  $\text{Ge}_{1-x}\text{Mn}_x\text{Te}$  monolayer under VCA. As expected, the Zeeman gaps  $\delta_z$  opened at both the valance band maximum (VBM) and Dirac point increase monotonically with the increasing Mn concentration (Fig. 1d), but the latter is an order of magnitude smaller than the former. This is due to the out-of-plane spin component of the electronic states near the Dirac point is smaller than that at the VBM, showing robustness against ferromagnetism. The reliability of VCA for  $\text{Ge}_{1-x}\text{Mn}_x\text{Te}$  monolayer is further confirmed by comparing the band structure obtained from using primitive cell of  $\text{Ge}_{0.98}\text{Mn}_{0.02}\text{Te}$  under VCA and  $7\times 7\times 1$  supercell of  $\text{Ge}_{48}\text{Mn}_1\text{Te}_{49}$  unfolded into the primitive cell (Fig. S3) [68]; the two agree well with each other. Moreover, the high-spin state of Mn dopants in the  $7\times 7\times 1$  supercell is found to possess lower total energy than the intermediate-spin state by about 62.6 meV.

*Superconductivity*—We next discuss the phonon mediated superconductivity of the 0.1-hole-doped GeTe monolayer. From the calculated phonon spectra (Fig. 2a), we first confirm its dynamical stability by the absence of imaginary frequency. For the acoustic branch with the lowest vibration frequency, Kohn anomalies can be seen at certain  $\mathbf{q}$ -points around  $\Gamma$ , which is favorable for enhancing electron-phonon coupling (EPC). The  $\mathbf{q}$ - and  $\nu$ -resolved EPC  $\lambda_{\mathbf{q}\nu}$  show two significant features (Fig. 2a). On one hand, all phonon modes can couple with electrons. This is further confirmed by the comparison between the phonon DOS  $F(\omega)$  and the isotropic Eliashberg spectral function  $\alpha^2F(\omega)$  (Fig. 2b). To estimate the relative contributions of acoustic and optical

modes, we calculated the cumulative EPC  $\lambda(\omega) = 2 \int_0^\omega d\omega' \frac{\alpha^2F(\omega')}{\omega'}$ . The  $\lambda(\omega)$

increases quickly to 0.92 at the frequency of  $\sim 10$  meV, which is about 83% of the total EPC  $\lambda=1.11$  (Fig. 2b). This indicates that the EPC stems mainly from the acoustic modes. On the other hand, only the vibration modes with a finite wave vector can couple with electrons. This is because for all the FS contours surrounding  $\Gamma$  (Fig. 1c), only a finite length of phonon wave vectors can connect the initial and final scattering states. Additionally, both  $\alpha^2F(\omega)$  and  $\lambda_{\mathbf{q}}$  illustrate that the soft modes associated with the Kohn anomalies help to enhance EPC.[80]

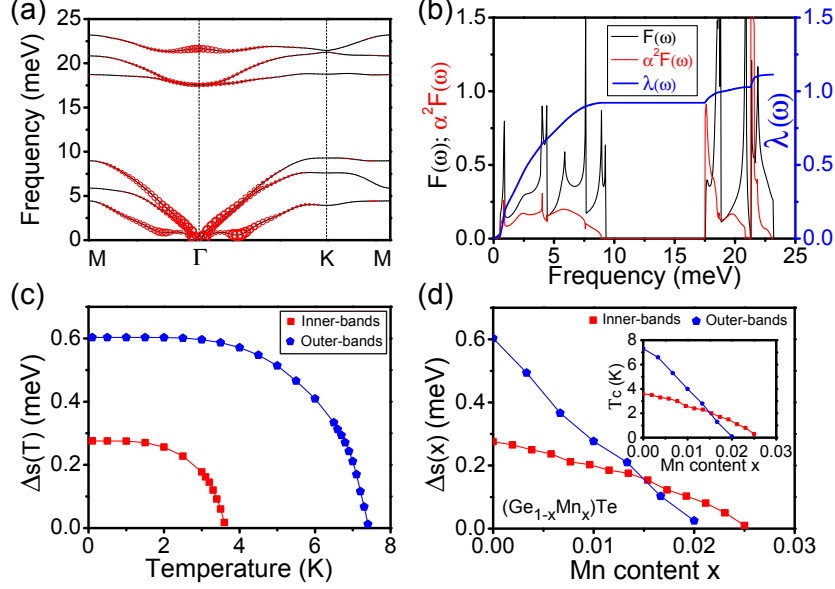


**Figure 2.** (a) Phonon spectra of the 0.1-hole-doped GeTe monolayer with the magnitude of EPC  $\lambda_{\mathbf{q}\nu}$  being drawn proportional to the size of red circles. (b) The plots of phonon DOS  $F(\omega)$ , Eliashberg spectral function  $\alpha^2 F(\omega)$ , and cumulative frequency-dependent EPC  $\lambda(\omega)$ . (c) The temperature-dependent superconducting gap  $\Delta_s(T)$  of the inner bands (red squares) and the outer bands (blue pentagons) of the 0.1-hole-doped GeTe monolayer. (d) The  $x$ -dependent superconducting gap  $\Delta_s(x)$  at 0.1 K and  $x$ -dependent  $T_c$  (inset) of the inner bands (red squares) and the outer bands (blue pentagons).

To estimate the superconducting transition temperature ( $T_c$ ) of GeTe monolayer, we construct a BdG Hamiltonian  $H_{BdG}(\mathbf{k})$  by employing the electronic Hamiltonian

$$H_{MLWFs}(\mathbf{k}):$$

$$H_{BdG}(\mathbf{k}) = \begin{pmatrix} H_{MLWFs}(\mathbf{k}) - \mu & \\ & -H_{MLWFs}^*(-\mathbf{k}) + \mu \end{pmatrix} + H_{\Delta_s} \quad (1)$$

$$H_{\Delta_s} = \Delta_s (\varphi_{i\uparrow}^\dagger \varphi_{(i+\frac{\mathbf{x}}{2})\downarrow}^\dagger - \varphi_{(i+\frac{\mathbf{x}}{2})\downarrow}^\dagger \varphi_{i\uparrow}^\dagger) + \Delta_s^* (\varphi_{(i+\frac{\mathbf{x}}{2})\downarrow} \varphi_{i\uparrow} - \varphi_{i\uparrow} \varphi_{(i+\frac{\mathbf{x}}{2})\downarrow}) \quad (2)$$

Here the basis of  $H_{MLWFs}(\mathbf{k})$  is the Maximally localized Wannier functions (MLWFs) and obtained by fitting the first-principles band structure of GeTe monolayer (Fig. S4a) using the WANNIER90-2.1 code [81] interfaced with QUANTUM ESPRESSO package [82]. Details can be seen from the SM [68].

Then the superconducting gap of GeTe monolayer can be calculated by numerically solving the following self-consistent gap equation [67]:

$$\Delta'_s = \frac{g}{2o\beta} \sum_{\mathbf{k}} \frac{\partial}{\partial \Delta_s} \ln[\text{Tr}(e^{-\beta H_{\text{BdG}}(\mathbf{k})})] \quad (3)$$

Here  $g=\lambda/N_F=1.07$  is the pairing strength and  $o$  is the number of atomic orbitals considered without considering spin degeneracy. Only the electronic states within one

Debye energy  $\Theta_D = \frac{\hbar\omega_D}{2\pi k_B}$  around Fermi level are summed over, which enables us to

estimate the superconductivity of specific bands by separately considering its FS contours, e.g. the inner-/outer-FS contours of inner/outer bands (Fig. S4b) [68]. By

assuming the Debye frequency  $\omega_D$  equals to the maximum of acoustic phonon

frequency  $\omega_{\text{max}}^a$  (Fig. 2a), we estimated a Debye energy  $\Theta_D \sim 1.475$  meV for GeTe monolayer.

The self-consistently calculated superconducting gap  $\Delta_s$  at different temperatures are shown in Fig. 2c. One can identify the two-gap feature of the 0.1-hole-doped GeTe monolayer and a similar trend of  $\Delta_s$  with increasing temperature as that of conventional SC. The  $\Delta_s$  at the zero-temperature limit is  $\sim 0.276$  ( $\sim 0.603$ ) meV and the  $T_c$  is around  $\sim 3.6$  ( $\sim 7.3$ ) K for the inner (outer) bands. The average gap ratio of  $2\Delta_s/(k_B T_c)$  is estimated to be  $\sim 1.85$ , which is smaller than the standard value ( $\sim 3.52$ ) of conventional SC [83,84], but remains within the reasonable range of previous experimental reports of GeTe [60]. We anticipate that the predicted 2D conventional superconductivity may be confirmed in the sonication-assisted liquid-phase exfoliated GeTe monolayer, spin-coated on the  $\text{SiO}_2$  substrate [65].

Next we simulate the superconductivity of Mn-doped GeTe ( $\text{Ge}_{1-x}\text{Mn}_x\text{Te}$ ) monolayer by adding an out-of-plane Zeeman energy  $B_z$  in  $H_{MLWFs}(\mathbf{k})$ :

$$H_{MLWFs}^z(\mathbf{k}) = B_z \sigma_z \otimes I_{\frac{\mathbf{n} \times \mathbf{n}}{2 \times 2}} + H_{MLWFs}(\mathbf{k}) \quad (4)$$

Here  $\sigma_z$  is the Pauli matrix in spin space and the  $I_{\frac{\mathbf{n} \times \mathbf{n}}{2 \times 2}}$  is a  $\frac{\mathbf{n}}{2} \times \frac{\mathbf{n}}{2}$  identity matrix.

By diagonalizing the  $H_{MLWFs}^z(\mathbf{k})$  for different  $B_z$  in momentum-space, we obtain the Zeeman gap  $\delta_z$  opened at the VBM and Dirac point (Fig. S5b) [68]. Comparing with the corresponding  $\delta_z$  (Fig. 1d) calculated by first-principles approach, one can estimate the relationship between the value of  $B_z$  and the concentration of Mn dopant  $x$ , which is  $x \sim 0.77B_z$  and  $x \sim 1.33B_z$  for the inner and outer bands, respectively. The self-consistently calculated  $\Delta_s$  and  $T_c$  (Fig. S5c and S5d) [68] demonstrate that they both decrease gradually with the increasing  $B_z$  due to the pairing breaking effect induced by

magnetism. The superconductivity of inner (outer) bands is fully superseded when  $B_z > 0.0325$  (0.015) eV, indicating their respective critical Mn doping concentration of  $x_c=0.025$  (0.02) (Fig. 2d). This value of  $x_c$  is comparable to that of 2% Mn doped  $\text{MgB}_2$ , [85] although the  $T_c$  of GeTe monolayer is one magnitude lower than  $\text{MgB}_2$ . Moreover, the two-gap feature is well preserved and the superconductivity of the inner bands is more robust against Mn doping than the outer bands. This can be attributed to the larger Zeeman gap opened in the VBM than at the Dirac point (Fig. 1d).

*Topological superconductivity and phase diagram.*—To realize TSC, another necessary pre-condition is that half of the Zeeman gap opened at the Dirac point of Rashba bands, i.e.  $\delta_z/2$ , is larger than the superconducting gap  $\Delta_s$  [27-29]. This condition is found to be met when  $x > x_{\min}=0.002$  (see comparison of  $\delta_z/2$  and  $\Delta_s$  in Fig. S6a [68]). We selected  $x \sim 0.006$  as an example to demonstrate the topological non-triviality of the superconducting  $\text{Ge}_{1-x}\text{Mn}_x\text{Te}$  monolayer, which is simulated by adding an out-of-plane Zeeman energy  $B_z \sim 7.5$  meV through equation (4). Having the superconducting gap of  $\sim 0.24$  meV (Fig. 2d), the specific  $H_{BdG}^z(\mathbf{k})$  of  $\text{Ge}_{0.994}\text{Mn}_{0.006}\text{Te}$  monolayer can be constructed via equation (1) and (2), which is analogous to the single-particle Hamiltonian of electrons with an energy gap mathematically.[86] By diagonalizing  $H_{BdG}^z(\mathbf{k})$  in the momentum space, we obtain the dispersion relation of superconducting quasiparticles (Fig. 3a). One can clearly see that the superconducting gap is indeed opened. Consequently, the topological invariant, i.e. first Chern number ( $N_c$ ), can be well-defined using the constructed  $H_{BdG}^z(\mathbf{k})$ .

For 2D systems, the Chern number of  $l$ -th band is calculated by integrating the Berry curvature  $\Omega^l(\mathbf{k})$  over the first BZ,  $N_c^l = \frac{1}{2\pi} \int_{BZ} \Omega^l(\mathbf{k}) d^2\mathbf{k}$ .  $\Omega^l(\mathbf{k}) = \nabla \times A^l(\mathbf{k})$ ,  $A^l(\mathbf{k}) = i \langle u^l(\mathbf{k}) | \partial_{\mathbf{k}} u^l(\mathbf{k}) \rangle$ , is the “field strength” of Berry connection. The total Chern number  $N_c$  can be obtained by summing up the Chern numbers of all the states below the superconducting gap, which is quantized to -1. The Berry curvature resides mainly at the  $\Gamma$  point associated with the Zeeman gap opening (Fig. 3b), similar to the band inversion in the quantum anomalous Hall systems. [87] Here we should emphasize that  $N_c$  does not physically correspond to a quantized Hall conductance because charge is not conserved in the BdG Hamiltonian. [88]



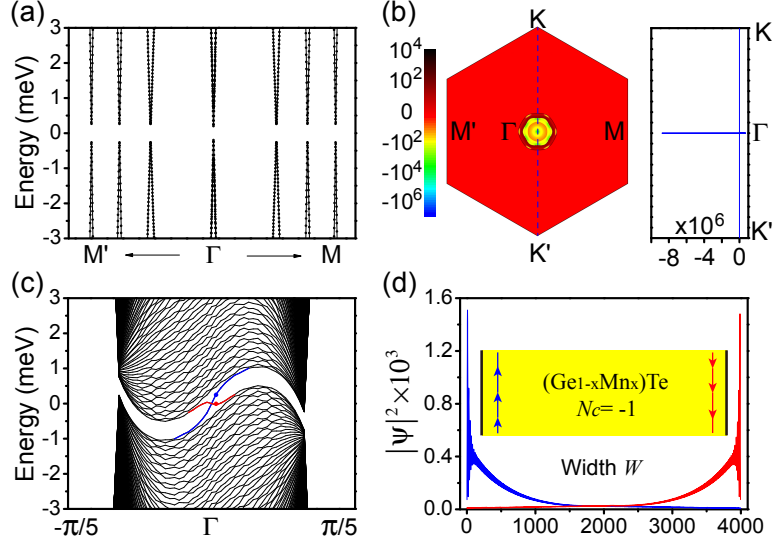


**Figure 3.** (a) The dispersion relation of quasiparticles calculated by the first-principles BdG Hamiltonian. (b) The distribution of total Berry curvatures for the states below the superconducting gap in the first BZ (left panel) and along the line of K- $\Gamma$ -K' (right panel). (c) The energy spectra of quasiparticles in a nanoribbon with the width ( $W$ ) of 4000 primitive cells. The chiral Majorana edge modes are highlighted by red and blue lines. (d) The spatial distributions of probability density  $|\psi|^2$  calculated from the wave function  $\psi$  of the in-gap states indicated by red and blue dot in (c). The inset is a schematic diagram of chiral Majorana edge modes with different propagation direction on opposite edges.

Based on the bulk-boundary correspondence, a TSC with Chern number  $N_c$  must have  $N_c$  edge states in the basis of chiral Majorana fermions. The BdG spectra of the nanoribbon with open boundary condition are plotted in Fig. 3c, which show two chiral Majorana edge modes residing in a continuous superconducting gap. The absence of a global gap in the spectra is attributed to the interplay between the intrinsic SOC and Zeeman field [89,90], leading to the formation of gapless TSC phase [91,92]. The spatial distributions of probability density  $|\psi|^2$  confirm the two modes localized at two different edges of the nanoribbon (Fig. 3d), consistent with the calculated Chern number. The inset of Fig. 3d shows a schematic diagram of the edge modes with the left (right) edge supporting a forward (backward) mover. The propagation of chiral Majorana fermions could lead to same unitary transformation as that in braiding Majorana zero modes, [93] and the deterministic creation and braiding of chiral edge vortices in hybrid structures were elaborated recently. [94] We anticipate that the chiral Majorana edge modes of  $\text{Ge}_{1-x}\text{Mn}_x\text{Te}$  monolayer can be detected using Josephson effect [95,96] or charge transport, [97-99] and controlled by magnetic flux. [100]

Based on the above results and analyses, we finally construct a phase diagram of the 0.1-hole-doped  $\text{Ge}_{1-x}\text{Mn}_x\text{Te}$  monolayer in Fig. 4, to help guide future experimental detection of the predicted TSC phase. At the zero-temperature limit, the SC phase will be preserved for  $x < x_c = 0.025$  and the TSC phase will arise when  $x > x_{\min} = 0.002$ , which are experimentally reachable [54-58]. At finite temperature, both the ferromagnetic and SC order should exist simultaneously for the formation of TSC phase. Referring to the ferromagnetic Curie temperatures of  $\text{Ge}_{1-x}\text{Mn}_x\text{Te}$  that increases linearly with increasing Mn concentration up to  $x=0.2$  and can be fit by  $T_c^{\text{FM}}(x)=333 \times x$  K (Fig. S6b) [54-58,68], we estimate  $T_c^{\text{FM}}(x)$  and  $T_c(x)$  will cross over at  $x' \sim 0.0085$  and temperature  $\sim 2.8$  K. Consequently, the TSC phase can be detected once the ferromagnetic order occurs for  $x < x'$ , while the SC order occurs first for  $x > x'$ . We suggest preparing the desired  $\text{Ge}_{1-x}\text{Mn}_x\text{Te}$  monolayer on  $\text{BaF}_2$  (111) [54-58] substrate by molecular beam epitaxy (MBE) since the growth is known to start in a 2D manner [58]. Meanwhile,  $\text{Ge}_{1-x}\text{Mn}_x\text{Te}$  thin film might also be used to detect the predicted TSC phase in surface by employing the potential gradient of an electric field, as done for the Ising SC  $\text{MoS}_2$ . [89,90]

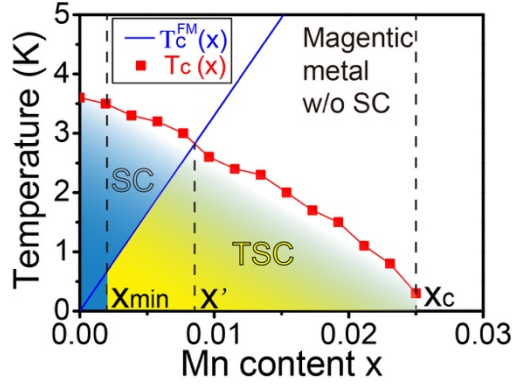


**Figure 4.** The schematic phase diagram of the 0.1-hole-doped  $\text{Ge}_{1-x}\text{Mn}_x\text{Te}$  monolayer in the parameter space of Mn doping concentration  $x$  and temperature. The yellow shaded region marks the TSC phase.

Lastly, in addition to the monolayer  $\text{Ge}_{1-x}\text{Mn}_x\text{Te}$  we demonstrated here, we suggest two more candidate materials for Class D TSC. First, it was theoretically reported a ferromagnetic order can be induced by hole doping in monolayer GaSe, attributed to the exchange splitting of electronic states that exhibit a sharp van Hove singularity below the Fermi level. [101] Given the superconductivity of bulk GaSe under pressure and Ga/GaSe layers being made experimentally, [102,103] the hole-doped monolayer GaSe is likely to be superconducting. Secondly, the magnetic order induced Rashba-Zeeman splitting in the Si-terminated surface of  $\text{HoRh}_2\text{Si}_2$  has been observed experimentally. [104] An spin-singlet Cooper pairing could be tunneled into this surface state by superconducting proximity effect. Our approach of first-principles BdG Hamiltonian may be applied to these systems in the near future.

## ACKNOWLEDGMENT

F.L. acknowledges financial support from DOE-BES (No. DE-FG02-04ER46148). X.Z. acknowledges financial support by China Postdoctoral Science Foundation (Grant No. 2017M620730). M.Z. acknowledge financial support from the National Natural Science Foundation of China (Nos. 21433006 and 11774201). K.J. acknowledges the support from Korea Research Fellowship Program through the National Research Foundation of Korea (NRF) funded by the Ministry of Science and ICT (Grant No. 2019H1D3A1A01071056).

## References

- [1] E. Majorana, *Il Nuovo Cimento* **14**, 171 (2008).
- [2] D. A. Ivanov, *Phys. Rev. Lett.* **86**, 268 (2001).
- [3] M. Stone and S.-B. Chung, *Phys. Rev. B* **73**, 014505 (2006).
- [4] C. Nayak, S. H. Simon, A. Stern, M. Freedman, and S. Das Sarma, *Rev. Mod. Phys.* **80**, 1083 (2008).
- [5] A. Y. Kitaev, *Ann. Phys.* **303**, 2 (2003).
- [6] G. E. Volovik, *J. Exp. Theor. Phys. Lett.* **70**, 609 (1999).
- [7] H. J. Kwon, K. Sengupta, and V. M. Yakovenko, *Eur. Phys. J. B* **37**, 349 (2004).
- [8] L. Jiang, D. Pekker, J. Alicea, G. Refael, Y. Oreg, and F. von Oppen, *Phys. Rev. Lett.* **107**, 236401 (2011).
- [9] S. Tewari, C. Zhang, S. Das Sarma, C. Nayak, and D.-H. Lee, *Phys. Rev. Lett.* **100**, 027001 (2008).
- [10] L. Fu, *Phys. Rev. Lett.* **104**, 056402 (2010).
- [11] Z. Wang, X.-L. Qi, and S.-C. Zhang, *Phys. Rev. B* **84**, 014527 (2011).
- [12] K. Nomura, S. Ryu, A. Furusaki, and N. Nagaosa, *Phys. Rev. Lett.* **108**, 026802 (2012).
- [13] K. Shiozaki and S. Fujimoto, *Phys. Rev. Lett.* **110**, 076804 (2013).
- [14] M. Sato and Y. Ando, *Rep. Prog. Phys.* **80**, 076501 (2017).
- [15] J. Alicea, *Rep. Prog. Phys.* **75**, 076501 (2012).
- [16] A. P. Mackenzie and Y. Maeno, *Rev. Mod. Phys.* **75**, 657 (2003).
- [17] Y. Maeno, S. Kittaka, T. Nomura, S. Yonezawa, and K. Ishida, *J. Phys. Soc. Jpn* **81**, 011009 (2011).
- [18] S. Sasaki and T. Mizushima, *Physica C* **514**, 206 (2015).
- [19] F. Kneidinger, E. Bauer, I. Zeiringer, P. Rogl, C. Blaas-Schenner, D. Reith, and R. Podloucky, *Physica C* **514**, 388 (2015).
- [20] E. Bauer and M. Sigrist, *Non-centrosymmetric superconductors: introduction and overview* (Springer Science & Business Media, 2012), Vol. 847.
- [21] N. Read and D. Green, *Phys. Rev. B* **61**, 10267 (2000).
- [22] A. Y. Kitaev, *Phys.-Usp.* **44**, 131 (2001).
- [23] M. Sato, *Phys. Lett. B* **575**, 126 (2003).
- [24] L. Fu and C. L. Kane, *Phys. Rev. Lett.* **100**, 096407 (2008).
- [25] R. M. Lutchyn, J. D. Sau, and S. Das Sarma, *Phys. Rev. Lett.* **105**, 077001 (2010).
- [26] Y. Oreg, G. Refael, and F. von Oppen, *Phys. Rev. Lett.* **105**, 177002 (2010).

- [27] M. Sato, Y. Takahashi, and S. Fujimoto, *Phys. Rev. Lett.* **103**, 020401 (2009).
- [28] J. D. Sau, S. Tewari, R. M. Lutchyn, T. D. Stanescu, and S. Das Sarma, *Phys. Rev. B* **82**, 214509 (2010).
- [29] J. D. Sau, R. M. Lutchyn, S. Tewari, and S. Das Sarma, *Phys. Rev. Lett.* **104**, 040502 (2010).
- [30] J.-P. Xu, M.-X. Wang, Z. L. Liu, J.-F. Ge, X. Yang, C. Liu, Z. A. Xu, D. Guan, C. L. Gao, D. Qian, Y. Liu, Q.-H. Wang, F.-C. Zhang, Q.-K. Xue, and J.-F. Jia, *Phys. Rev. Lett.* **114**, 017001 (2015).
- [31] H.-H. Sun, K.-W. Zhang, L.-H. Hu, C. Li, G.-Y. Wang, H.-Y. Ma, Z.-A. Xu, C.-L. Gao, D.-D. Guan, Y.-Y. Li, C. Liu, D. Qian, Y. Zhou, L. Fu, S.-C. Li, F.-C. Zhang, and J.-F. Jia, *Phys. Rev. Lett.* **116**, 257003 (2016).
- [32] W. Yu, W. Pan, D. L. Medlin, M. A. Rodriguez, S. R. Lee, Z.-q. Bao, and F. Zhang, *Phys. Rev. Lett.* **120**, 177704 (2018).
- [33] J. Wiedenmann, E. Bocquillon, R. S. Deacon, S. Hartinger, O. Herrmann, T. M. Klapwijk, L. Maier, C. Ames, C. Brüne, C. Gould, A. Oiwa, K. Ishibashi, S. Tarucha, H. Buhmann, and L. W. Molenkamp, *Nat. Commun.* **7**, 10303 (2016).
- [34] R. M. Lutchyn, E. P. A. M. Bakkers, L. P. Kouwenhoven, P. Krogstrup, C. M. Marcus, and Y. Oreg, *Nat. Rev. Mater.* **3**, 52 (2018).
- [35] T. Uchihashi, *Nanotechnology* **26**, 344004 (2015).
- [36] C. Lei, H. Chen, and A. H. MacDonald, *Phys. Rev. Lett.* **121**, 227701 (2018).
- [37] L. Kuerten, C. Richter, N. Mohanta, T. Kopp, A. Kampf, J. Mannhart, and H. Boschker, *Phys. Rev. B* **96**, 014513 (2017).
- [38] X.-X. Gong, H.-X. Zhou, P.-C. Xu, D. Yue, K. Zhu, X.-F. Jin, H. Tian, G.-J. Zhao, T.-Y. Chen, *Chin. Phys. Lett.* **32**, 067402 (2015).
- [39] N. Mohanta and A. Taraphder, *EPL* **108**, 60001 (2014).
- [40] F. Loder, A. P. Kampf, and T. Kopp, *Sci. Rep.* **5**, 15302 (2015).
- [41] N. Mohanta and A. Taraphder, *Phys. Rev. B* **92**, 174531 (2015).
- [42] X. Gong, M. Kargarian, A. Stern, D. Yue, H. Zhou, X. Jin, V. M. Galitski, V. M. Yakovenko, and J. Xia, *Sci. Adv.* **3**, e1602579 (2017).
- [43] J. Wang, X. Gong, G. Yang, Z. Lyu, Y. Pang, G. Liu, Z. Ji, J. Fan, X. Jing, C. Yang, F. Qu, X. Jin, and L. Lu, *Phys. Rev. B* **96**, 054519 (2017).
- [44] S.-P. Chao, *Phys. Rev. B* **99**, 064504 (2019).
- [45] P. Chauhan, F. Mahmood, D. Yue, P.-C. Xu, X. Jin, and N. P. Armitage, *Phys. Rev. Lett.* **122**, 017002 (2019).
- [46] R. Ghadimi, M. Kargarian, and S. A. Jafari, *Phys. Rev. B* **100**, 024502 (2019).
- [47] Z. Wang, P. Zhang, G. Xu, L. K. Zeng, H. Miao, X. Xu, T. Qian, H. Weng, P. Richard, A. V. Fedorov, H. Ding, Xi Dai, and Z. Fang, *Phys. Rev. B* **92**, 115119 (2015).
- [48] Z. F. Wang, H. Zhang, D. Liu, C. Liu, C. Tang, C. Song, Y. Zhong, J. Peng, F. Li, C. Nie, L. Wang, X. J. Zhou, X. Ma, Q. K. Xue, and F. Liu, *Nat. Mater.* **15**, 968 (2016).
- [49] J.-F. Zhang, P.-J. Guo, M. Gao, K. Liu, and Z.-Y. Lu, *Phys. Rev. B* **99**, 045110 (2019).
- [50] P.-J. Guo, J.-F. Zhang, H.-C. Yang, Z.-X. Liu, K. Liu, and Z.-Y. Lu, arXiv preprint arXiv:1811.06401 (2018).
- [51] K.-H. Jin, H. Huang, J.-W. Mei, Z. Liu, L.-K. Lim, and F. Liu, *npj Comput. Mater.*

- 5, 57 (2019).
- [52] M. Kim, C.-Z. Wang, and K.-M. Ho, *Phys. Rev. B* **99**, 224506 (2019).
- [53] R. W. Cochrane, M. Plischke, and J. O. Ström-Olsen, *Phys. Rev. B* **9**, 3013 (1974).
- [54] W. Q. Chen, K. L. Teo, M. B. A. Jalil, and T. Liew, *J. Appl. Phys.* **99**, 08D515 (2006).
- [55] W. Q. Chen, S. T. Lim, C. H. Sim, J. F. Bi, K. L. Teo, T. Liew, and T. C. Chong, *J. Appl. Phys.* **104**, 063912 (2008).
- [56] Y. Fukuma, H. Asada, S. Miyawaki, T. Koyanagi, S. Senba, K. Goto, and H. Sato, *Appl. Phys. Lett.* **93**, 252502 (2008).
- [57] Y. Fukuma, K. Goto, S. Senba, S. Miyawaki, H. Asada, T. Koyanagi, and H. Sato, *J. Appl. Phys.* **103**, 053904 (2008).
- [58] M. Hassan, G. Springholz, R. T. Lechner, H. Groiss, R. Kirchschrager, and G. Bauer, *J. Cryst. Growth* **323**, 363 (2011).
- [59] R. A. Hein, J. W. Gibson, R. Mazelsky, R. C. Miller, and J. K. Hulm, *Phys. Rev. Lett.* **12**, 320 (1964).
- [60] J. L. Smith and P. J. Stiles, *J. Low Temp. Phys.* **26**, 101 (1977).
- [61] T. Chattopadhyay, J. X. Boucherle, and H. G. vonSchnering, *J. Phys. C* **20**, 1431 (1987).
- [62] K. M. Rabe and J. D. Joannopoulos, *Phys. Rev. B* **36**, 6631 (1987).
- [63] J. Krempaský, S. Muff, F. Bisti, M. Fanciulli, H. Volfová, A. P. Weber, N. Pilet, P. Warnicke, H. Ebert, J. Braun, F. Bertran, V. V. Volobuev, J. Minár, G. Springholz, J. H. Dil, and V. N. Strocov, *Nat. Commun.* **7**, 13071 (2016).
- [64] R. Yoshimi, K. Yasuda, A. Tsukazaki, K. S. Takahashi, M. Kawasaki, and Y. Tokura, *Sci. Adv.* **4**, eaat9989 (2018).
- [65] P. Zhang, F. Zhao, P. Long, Y. Wang, Y. Yue, X. Liu, Y. Feng, R. Li, W. Hu, Y. Li, and W. Feng, *Nanoscale* **10**, 15989 (2018).
- [66] M. Qiao, Y. Chen, Y. Wang, and Y. Li, *J. Mater. Chem. A* **6**, 4119 (2018).
- [67] C. Wang, B. Lian, X. Guo, J. Mao, Z. Zhang, D. Zhang, B.-L. Gu, Y. Xu, and W. Duan, *Phys. Rev. Lett.* **123**, 126402 (2019).
- [68] See Supplemental Material at <http> for computational details and supplemental Figures.
- [69] S. LaShell, B. A. McDougall, and E. Jensen, *Phys. Rev. Lett.* **77**, 3419 (1996).
- [70] Y. M. Koroteev, G. Bihlmayer, J. E. Gayone, E. V. Chulkov, S. Blügel, P. M. Echenique, and P. Hofmann, *Phys. Rev. Lett.* **93**, 046403 (2004).
- [71] W. Ming, Z. F. Wang, M. Zhou, M. Yoon, and F. Liu, *Nano Letters* **16**, 404 (2016).
- [72] M. Liebmann, C. Rinaldi, D. D. Sante, J. Kellner, C. Pauly, R. N. Wang, J. E. Boschker, A. Giussani, S. Bertoli, M. Cantoni, L. Baldrati, M. Asa, I. Vobornik, G. Panaccione, D. Marchenko, J. S.-Barriga, O. Rader, R. Calarco, S. Picozzi, R. Bertacco, and M. Morgenstern, *Adv. Mater.* **28**, 560 (2016).
- [73] J. Krempaský, H. Volfová, S. Muff, N. Pilet, G. Landolt, M. Radović, M. Shi, D. Kriegner, V. Holý, J. Braun, H. Ebert, F. Bisti, V. A. Rogalev, V. N. Strocov, G. Springholz, J. Minár, and J. H. Dil, *Phys. Rev. B* **94**, 205111 (2016).
- [74] A. C. Potter and P. A. Lee, *Phys. Rev. B* **83**, 184520 (2011).
- [75] H. Przybylińska, G. Springholz, R. T. Lechner, M. Hassan, M. Wegscheider, W.

- Jantsch, and G. Bauer, Phys. Rev. Lett. **112**, 047202 (2014).
- [76] K. Leung, S. B. Rempe, P. A. Schultz, E. M. Sproviero, V. S. Batista, M. E. Chandross, and C. J. Medforth, J. Am. Chem. Soc. **128**, 3659 (2006).
- [77] L. Nordheim, Ann. Phys. **401**, 607 (1931).
- [78] M. Inoue, H. Yagi, T. Tatsukawa, and Y. Kaku, J. Phys. Soc. Jpn **45**, 1610 (1978).
- [79] Y. Fukuma, H. Asada, N. Nishimura, and T. Koyanagi, J. Appl. Phys. **93**, 4034 (2003).
- [80] C. Si, Z. Liu, W. Duan, and F. Liu, Phys. Rev. Lett. **111**, 196802 (2013).
- [81] A. A. Mostofi, J. R. Yates, Y.-S. Lee, I. Souza, D. Vanderbilt, and N. Marzari, Comput. Phys. Commun. **178**, 685 (2008).
- [82] P. Giannozzi, S. Baroni, N. Bonini, M. Calandra, R. Car, C. Cavazzoni, D. Ceresoli, G. L. Chiarotti, M. Cococcioni, I. Dabo *et al.*, J. Phys.-Condens. Mat. **21**, 395502 (2009).
- [83] C. J. David, Supercond. Sci. Tech. **26**, 115011 (2013).
- [84] J. Bardeen, L. N. Cooper, and J. R. Schrieffer, Physical Review **108**, 1175 (1957).
- [85] K. Rogacki, B. Batlogg, J. Karpinski, N. D. Zhigadlo, G. Schuck, S. M. Kazakov, P. Wägli, R. Puźniak, A. Wiśniewski, F. Carbone, A. Brinkman, and D. van der Marel, Phys. Rev. B **73**, 174520 (2006).
- [86] A. P. Schnyder, S. Ryu, A. Furusaki, and A. W. W. Ludwig, Phys. Rev. B **78**, 195125 (2008).
- [87] X. Zhang, Z. Wang, M. Zhao, and F. Liu, Phys. Rev. B **93**, 165401 (2016).
- [88] X.-L. Qi, T. L. Hughes, and S.-C. Zhang, Phys. Rev. B **82**, 184516 (2010).
- [89] J. M. Lu, O. Zheliuk, I. Leermakers, N. F. Q. Yuan, U. Zeitler, K. T. Law, and J. T. Ye, Science **350**, 1353 (2015).
- [90] Y. Saito, Y. Nakamura, M. S. Bahramy, Y. Kohama, J. Ye, Y. Kasahara, Y. Nakagawa, M. Onga, M. Tokunaga, T. Nojima, Y. Yanase, and Y. Iwasa, Nat. Phys. **12**, 144 (2016).
- [91] C. L. M. Wong, J. Liu, K. T. Law, and P. A. Lee, Phys. Rev. B **88**, 060504 (2013).
- [92] F. Loder, A. P. Kampf, and T. Kopp, Sci. Rep. **5**, 15302 (2015).
- [93] B. Lian, X.-Q. Sun, A. Vaezi, X.-L. Qi, and S.-C. Zhang, P. Natl. Acad. Sci. USA **115**, 10938 (2018).
- [94] C. W. J. Beenakker, P. Baireuther, Y. Herasymenko, I. Adagideli, L. Wang, and A. R. Akhmerov, Phys. Rev. Lett. **122**, 146803 (2019).
- [95] Y. Tanaka, T. Yokoyama, and N. Nagaosa, Phys. Rev. Lett. **103**, 107002 (2009).
- [96] C.-A. Li, J. Li, and S.-Q. Shen, Phys. Rev. B **99**, 100504 (2019).
- [97] L. Fu and C. L. Kane, Phys. Rev. Lett. **102**, 216403 (2009).
- [98] S. B. Chung, X.-L. Qi, J. Maciejko, and S.-C. Zhang, Phys. Rev. B **83**, 100512 (2011).
- [99] Q. L. He, L. Pan, A. L. Stern, E. C. Burks, X. Che, G. Yin, J. Wang, B. Lian, Q. Zhou, E. S. Choi, K. Murata, X. Kou, Z. Chen, T. Nie, Q. Shao, Y. Fan, S.-C. Zhang, K. Liu, J. Xia, and K. L. Wang, Science **357**, 294 (2017).
- [100] Y.-F. Zhou, Z. Hou, P. Lv, X. Xie, and Q.-F. Sun, Sci. China Phys. Mech. **61**, 127811 (2018).
- [101] T. Cao, Z. Li, and S. G. Louie, Phys. Rev. Lett. **114**, 236602 (2015).
- [102] K. J. Dunn and F. P. Bundy, Appl. Phys. Lett. **36**, 709 (1980).

- [103] W. Desrat, M. Moret, O. Briot, T. H. Ngo, B. A. Piot, B. Jabakhanji, and B. Gil, *Mater. Res. Express* **5**, 045901 (2018).
- [104] A. Generalov, M. M. Otkov, A. Chikina, K. Kliemt, K. Kummer, M. Höppner, M. Güttler, S. Seiro, A. Fedorov, S. Schulz *et al.*, *Nano Lett.* **17**, 811 (2017).